Int. J. Heat Mass Transfer. Vol. 34, No. 7, pp. 1617–1631, 1991
Printed in Great Britain

0017–9310/91 $3.00 + 0.00

Measurements of turbulent heat transport in a boundary layer with an embedded streamwise vortex

DONALD E. WROBLEWSKI and PAMELA A. EIBECK
Mechanical Engineering Department, University of California, Berkeley, CA 94027, U.S.A.

(*Received* 25 *May* 1990 *and in final form* 8 *August* 1990)

Abstract—All three components of the turbulent heat flux vector ($\overline{u\theta}$, $\overline{v\theta}$, and $\overline{w\theta}$) and most of the components of the Reynolds stress tensor are measured in a boundary layer disturbed by an embedded streamwise vortex. Some similarities are observed between the cross-plane heat fluxes ($\overline{v\theta}$ and $\overline{w\theta}$) and the analogous Reynolds stress terms ($\overline{uv}$ and $\overline{uw}$). However, the vortex interaction with the boundary layer seems to enhance heat transport more than momentum transport, especially in the vicinity of the vortex core. The cross-plane heat transport vector, formed from $\overline{v\theta}$ and $\overline{w\theta}$, is nearly perpendicular to the isotherms at all points, suggesting that an isotropic eddy-diffusivity model would be suitable for this flow.

INTRODUCTION

When a streamwise vortex interacts with an otherwise two-dimensional boundary layer, the result is a complex three-dimensional flow characterized by moderate secondary velocities that enhance mixing of near-wall fluid with the free stream. The most common practical application is the introduction of the vortex into a boundary layer to suppress separation. These flows also occur naturally when horseshoe vortices form near the junction of a blunt body and a wall on which a turbulent boundary layer is developing. A typical example is the junction between a gas-turbine blade and its endwall, where the enhanced mixing due to the vortices can lead to locally high heat-transfer rates along the endwall.

This paper reports the results of a detailed study of the turbulent heat transport within a boundary layer disturbed by a streamwise vortex. Understanding the mechanisms for turbulent heat transport in this three-dimensional flow can help improve turbulence models and provide insights into general passive-scalar transport in complex flows.

Recent studies of interactions between vortices and boundary layers have concentrated on characterizing the transport mechanisms of momentum and turbulent kinetic energy, with the hopes of improving turbulence modeling and prediction techniques for these complex flows. Shabaka *et al.* [1] measured the Reynolds stresses and turbulent triple products in a flow with a single embedded streamwise vortex generated in the contraction section of the wind tunnel. The structure of the turbulence was greatly altered in the vicinity of the vortex, as evidenced by the large variations in the shear stress/turbulent kinetic energy ratio, a_1, and the shear-stress correlation coefficients. The Reynolds shear-stress contours generally followed the principle that momentum fluxes follow the gradient of the mean momentum. Mehta *et al.* [2] also reported on similar studies for boundary layers with a pair of vortices with common flow upwards and for a pair with common flow downwards. The Reynolds shear stresses seemed to follow the concept of an eddy viscosity in all cases, but the complex nature of the resulting eddy-viscosity contours led to the conclusion that simple algebraic models would not be sufficient for these flows. Westphal *et al.* [3] investigated the effect of an adverse pressure gradient on a single embedded vortex, and found that the presence of the pressure gradient caused greater distortion of the Reynolds stress profiles and caused greater diffusion of the vortex into the surrounding flow.

Some studies have included mean-temperature measurements to study the local wall heat-transfer effects and the thermal boundary-layer characteristics. A single vortex was studied in ref. [4] and it was found that the Stanton number was increased by up to 20% in the downwash region due to the thinning of the thermal boundary layer, and correspondingly decreased in the upwash region where the thermal boundary layer was thickened. It was postulated that essentially two-dimensional mechanisms controlled the heat transfer in the near-wall region for the weak vortices studied. Pauley and Eaton [5] found that, with vortex pairs, the two-dimensional similarity breaks down when secondary flow angles are greater than 10 deg. In these regions, the wall heat-transfer rates could be correlated with the turbulence intensity near the wall.

The turbulent transport of heat is characterized by the Reynolds heat-flux terms ($\overline{v\theta}$, $\overline{w\theta}$, and $\overline{u\theta}$) which appear in the Reynolds averaged energy equation

$$\bar{U}\frac{\partial \bar{T}}{\partial x}+\bar{V}\frac{\partial \bar{T}}{\partial y}+\bar{W}\frac{\partial \bar{T}}{\partial z}=-\frac{\partial}{\partial x}\left(\overline{u\theta}-\alpha\frac{\partial \bar{T}}{\partial x}\right)-\frac{\partial}{\partial y}\left(\overline{v\theta}-\alpha\frac{\partial \bar{T}}{\partial y}\right)-\frac{\partial}{\partial z}\left(\overline{w\theta}-\alpha\frac{\partial \bar{T}}{\partial z}\right) \quad (1)$$

NOMENCLATURE

A	calibration constant in equation (4)
a_1	turbulent shear stress/kinetic energy ratio, $\lvert\tau\rvert/k^2$
a_θ	heat-flux structure parameter, $[(\overline{v\theta})^2+(\overline{w\theta})^2]^{1/2}/[(\theta')^2k^2]^{1/2}$
B	calibration constant in equation (4)
c_p	specific heat [kJ kg^{-1} °C^{-1}]
d	diameter of hot-wire sensor [m]
$\mathscr{D}_{ij}$	eddy-diffusivity tensor [m^2 s^{-1}]
E_{wi}	voltage measured across wire [V]
$\hat{j},\hat{k}$	unit vectors in the y- and z-directions
$\frac{1}{2}k^2$	turbulent kinetic energy per unit mass [m^2 s^{-2}]
l	active length of hot-wire sensor [m]
m,n	exponents for hot-wire calibration, equation (4)
$\mathscr{P}_{ij}$	turbulent Prandtl number tensor, equation (17)
Pr_t	scalar turbulent Prandtl number, $\varepsilon_M/\varepsilon_H$
q_w	wall heat flux [W m^{-2}]
Re_{δ_2}	momentum-thickness Reynolds number, $U_\infty\delta_2/\nu$
St	Stanton number, $q_w/[\rho c_p U_\infty(T_w-T_\infty)]$
T	instantaneous temperature [°C]
$\bar{T}$	time-average temperature [°C]
u_τ	friction velocity [m s^{-1}]
U_{eff}	effective cooling velocity of hot wire [m s^{-1}]
U,V,W	instantaneous velocity components [m s^{-1}]
$\bar{U},\bar{V},\bar{W}$	time-average velocity components [m s^{-1}]
u,v,w	fluctuating velocity components [m s^{-1}]
u',v',w'	r.m.s. velocities [m s^{-1}]
$\overline{u\theta}$	longitudinal component of turbulent heat flux [m s^{-1} °C]
$\overline{uv}$, $\overline{uw}$, $\overline{vw}$	Reynolds shear stresses [(m s^{-1})^2]
$\overline{v\theta}$	normal component of turbulent heat flux [m s^{-1} °C]
$\mathscr{V}_{ij}$	eddy-viscosity tensor [m^2 s^{-1}]
$\overline{w\theta}$	spanwise component of turbulent heat flux [m s^{-1} °C]
x	streamwise distance in boundary layer, measured from trip [m]
y	vertical distance measured from wall upwards [m]
z	spanwise distance in boundary layer, measured from centerline [m].

Greek symbols

α	molecular thermal diffusivity [m^2 s^{-1}]
Γ	circulation of vortex [m^2 s^{-1}]
δ_{loc}	0.99 momentum boundary-layer thickness at a given z location [m]
δ_2	momentum thickness of boundary layer, $\int_0^\infty(\bar{U}/U_\infty)(1-(\bar{U}/U_\infty))\,dy$ [m]
$\delta_{2\text{-d}}$	0.99 momentum boundary-layer thickness for undisturbed two-dimensional boundary layer [m]
Δ	0.99 thermal boundary-layer thickness [m]
ε_H	eddy diffusivity [m^2 s^{-1}]
ε_M	eddy viscosity [m^2 s^{-1}]
θ	temperature fluctuation [°C]
θ'	r.m.s. temperature [°C]
ν	molecular viscosity [m^2 s^{-1}]
ρ	density [kg m^{-3}]
τ	turbulent shear stress [N m^{-2}]
ψ_{eff}	effective cooling angle of hot wire [deg]
Ω_x	streamwise vorticity, $(\partial\bar{W}/\partial y-\partial\bar{V}/\partial z)$ [s^{-1}].

Subscripts

i,j,k	integers used in index notation relations
m	mean value between hot wire and air
meas	measured value
wi	condition at the hot-wire sensor
w	condition at the wall
∞	condition in the free stream.

where θ represents the temperature fluctuation and $\bar{T}$ the mean temperature. Physically, the Reynolds heat-flux terms represent the convective transport of heat due to the turbulent fluctuations, but are usually grouped with molecular heat-flux terms, in a manner analogous to the Reynolds stress terms in the momentum equation. In two-dimensional boundary layers, this is convenient for defining an eddy diffusivity

$$\varepsilon_H = -\frac{\overline{v\theta}}{\partial\bar{T}/\partial y} \tag{2}$$

and a turbulent Prandtl number

$$Pr_t = \frac{\overline{uv}\partial\bar{T}/\partial y}{\overline{v\theta}\partial\bar{U}/\partial y} \tag{3}$$

both of which are useful quantities in turbulence modeling.

Early experimental investigations of turbulent heat transfer in boundary layers used an indirect method to determine the turbulent heat flux and the turbulent Prandtl number. In a two-dimensional flow, only the second term on the right-hand side of equation (1) is significant. By measuring the mean temperatures and velocities, all of the terms on the left-hand side can be determined and the turbulent heat flux is then found by integration across the boundary layer. A similar approach is used to find $\overline{uv}$ using the momentum equation. Compilations of the turbulent Prandtl number from these early studies were presented by Blom [6]

and Kestin and Richardson [7], and these showed a wide scatter from 0.1 to 2.0 in a two-dimensional boundary layer.

Direct measurement of the turbulent heat flux requires simultaneous measurements of temperature and velocities, usually with hot-wire anemometry techniques. Pioneering measurements of $\overline{v\theta}$ and Pr_t for air by Johnson [8], and later by Blom [6], in boundary layers with a step change in wall temperature showed the turbulent Prandtl number to be between 0.8 and 1.2 in the outer region of the thermal boundary layer. Several studies on constant wall temperature, two-dimensional boundary layers with pressure gradients, transpiration, and surface roughness [9–11] revealed that the turbulent Prandtl number was dependent upon boundary conditions and flow parameters. An adverse pressure gradient generally decreased Pr_t in the log region and the outer region, while suction increased it.

Perry and Hoffman [12] studied the instantaneous (as opposed to the time average) heat and momentum fluxes in a constant wall temperature boundary layer in which the temperature and momentum boundary layers had the same virtual origin. They found that the 'sweeps' and 'bursts' of Reynolds stresses were generally accompanied by equivalent occurrences in $\overline{v\theta}$.

Antonia *et al.* [13] measured the turbulent heat flux in the region downstream of a step change in wall heat flux, and found that $\overline{v\theta}$ profiles showed similarity when y was normalized on the local temperature boundary-layer thickness. The turbulent Prandtl number was found to be greater than unity in the inner region of the thermal layer, even at the furthest downstream station. Subramanian and Antonia [14] later studied the effects of Reynolds number on boundary layers with constant wall heat flux, and the same virtual origin for the momentum and thermal boundary layers. They found that similarity in $\overline{v\theta}$ profiles could be obtained for $Re_{\delta_2} > 4750$. For lower Reynolds numbers, they could not explain significantly low values of $\overline{v\theta}$ near the wall. The turbulent Prandtl number effect was difficult to determine due to the unavoidably high uncertainty.

Studies of turbulent heat flux in boundary layers with wall curvature have revealed differences between heat and momentum transport in flows that are more complex than the two-dimensional boundary layer. Gibson and Verriopoulos [15] found that the turbulent heat flux and the Stanton numbers were more sensitive to changes in wall curvature than the Reynolds stresses and the skin friction. Kim and Simon [16] investigated the effects of free-stream turbulence intensity and recovery on the turbulent heat transport in boundary layers with wall curvature. In the recovery region, they found that $\overline{v\theta}$ often overshot its flat-plate levels. For higher free-stream turbulence levels, $\overline{uv}$ showed a reversal in sign, while $\overline{v\theta}$ did not, indicating a breakdown in the usual analogies between heat and momentum transport.

The purpose of this paper is to present measurements of all three components of the Reynolds heat-flux vector in a boundary layer with a single embedded streamwise vortex. These data, presented here for one set of operating conditions and one streamwise location, will provide some initial observations on passive-scalar transport in complex three-dimensional flows. This will augment the growing body of data on the turbulent transport of active components (e.g. momentum, kinetic energy and Reynolds stresses) in these flows, and provide information for turbulence modelers who are interested specifically in predicting passive-scalar transport and heat transfer. The results represent some of the first measurements of the spanwise component of heat flux, $\overline{w\theta}$, in boundary-layer flows.

EXPERIMENTAL APPROACH

Experimental facility

The convection boundary layer facility used in this study is described in detail in ref. [17]. The working section of the facility, shown in Fig. 1, consists of four sections: (1) a 122 cm long heated development section, (2) a 26 cm long unheated removable hatch for holding the vortex generators, (3) a 157 cm long heated test section, and (4) a 61 cm long exit section. All heaters were operated with a constant power input, which approximated a constant wall heat-flux boundary condition.

The vortex generator is a half-delta wing, 5.9 cm long and 2.7 cm high at its base, and is positioned at an angle-of-attack of 12 deg. The trailing edge of the vortex generator is located along the centerline of the tunnel, 1.36 m downstream of the boundary-layer trip. Here, the local boundary-layer thickness was approximately the same as the vortex generator height. Measurements were taken across the y–z plane located 2.65 m from the boundary-layer trip.

Probes

Two triple-wire probes were developed to measure turbulent heat flux in three-dimensional flows. Each probe consists of two constant-temperatures hot wires in a X-wire configuration, with a constant-current cold wire located in between and in a plane parallel to the X-wire sensors. The sensors of the uv probe are oriented vertically, so that the X-wire measures the U and V components of velocity and the cold wire measures the temperature, T. The sensors of the uw probe are oriented horizontally, rotated 90 deg from the uv configuration, so that the X-wire measures the U and W components of velocity.

All three sensors of the heat-flux probes are 2.5 μm diameter tungsten, with $l/d = 280$. The wire ends are plated with 24 μm diameter copper plating, which extends the overall wire length to 3.3 mm for the X-wire sensors, and to 2.2 mm for the cold wire. An analytical technique was developed to compensate for

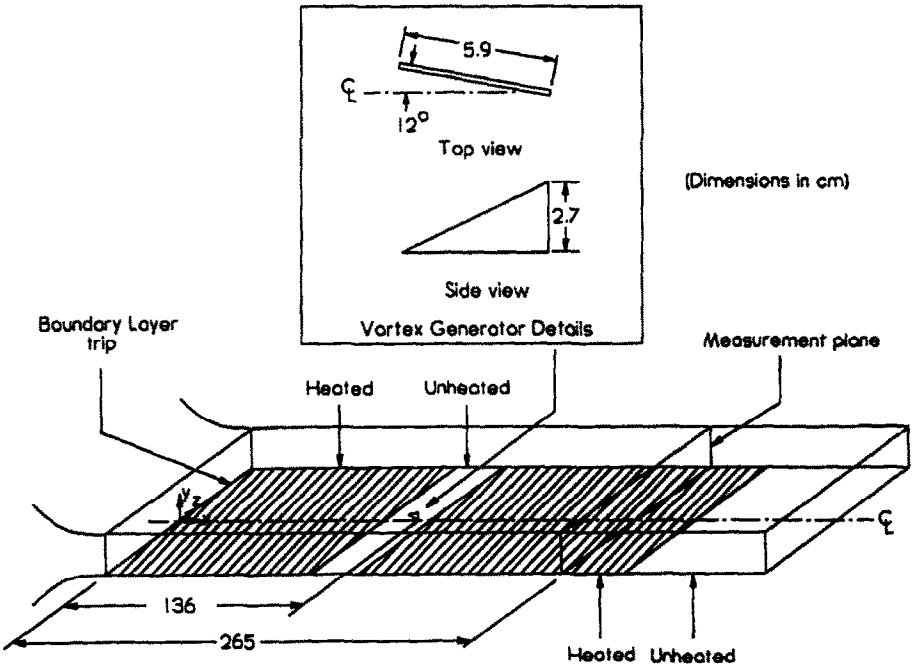

FIG. 1. Working section of the convective boundary-layer facility.

the reduced frequency response of the constant-current cold wire, accounting for both end-conduction and wire thermal-inertia effects. Details of this technique and the qualification of the probes in a two-dimensional boundary layer can be found in ref. [17].

A single wire, 1 μm platinum probe (TSI model 1218-P0.5) with $l/d = 420$ was used as a constant-current cold wire to also measure mean temperatures. This probe was used to obtain measurements closer to the wall ($y = 0.13$ mm) than were possible with the heat-flux probe.

Data acquisition

The heat-flux-probe X-wires were operated by DISA 56C17/56C01 constant temperature anemometer (CTA) systems. Square-wave tests indicated a 3 dB cutoff frequency for the system of 6500 Hz. A DISA 56C20 temperature bridge used in conjunction with the 56C01 CTA module provided a constant-current system for the cold wires. DISA model 56NCN signal conditioners connected to the anemometer outputs provided adjustable gain, low-pass filtering, and high-pass filtering. The signal-conditioner outputs, unlinearized in the case of the hot wires, were digitized using a Data Translation 2828 high-speed data-acquisition board in a Data Translation CyClone JS 286 microcomputer. The A/D board featured simultaneous sample and hold, which allowed each channel to be sampled within 5 ns. For mean and correlation measurements, data was sampled at 6000 Hz per channel for 5.5 s. Raw data was stored in extended memory buffers within the microcomputer, transferred to the hard disk for data reduction, and then archived on a Colorado Memory Systems DJ-10 streaming-tape backup drive. The data was then reduced computationally, using the computer.

The measurements were obtained across the y–z plane in three steps. First, the uv probe was used to obtain measurements of $\bar{U}$, $\bar{V}$, $(u')^2$, $(v')^2$, $(\theta')^2$, $\overline{uv}$, $\overline{v\theta}$, and $\overline{u\theta}$ at all the desired locations. Second, the uw probe was used to measure $\bar{U}$, $\bar{W}$, $(u')^2$, $(w')^2$, $(\theta')^2$, $\overline{uw}$, $\overline{w\theta}$, and $\overline{u\theta}$ at the same locations. Finally, the platinum cold wire was used to additionally measure $\bar{T}$ on a finer grid to allow for near wall measurements and for more accurate determinations of the temperature gradients, needed for determining the eddy diffusivities. The traversing system which was used had a precision of 0.00125 mm per cm of travel, which allowed for repositioning the various probes with only a small uncertainty. This approach did not allow for the measurement of the $\overline{vw}$ Reynolds stress. Although this term may be important when considering streamwise vorticity development, it was decided that it was only secondary to the main objective of this study, which was the measurement of the Reynolds heat-flux terms.

Data reduction

The hot-wire sensors, which form the X-wire component of the heat-flux probe, are calibrated by placing the probe in a separate laminar-jet calibration

facility and varying the temperature and velocity of the jet. The data is fit to a calibration equation that is obtained from a modified form of the Collis and Williams equation [18]

$$U_{\text{eff}} = \left[A\left(\frac{T_m}{T}\right)^m \frac{T_m^{(1.76n-0.8)}}{(T_{wi}-T)} E_{wi}^2 + BT_m^{1.76n} \right]^{1/n} \quad (4)$$

where E_{wi} is the voltage across the wire, T_{wi} the wire temperature, T the air temperature, $T_m = (T_{wi}+T)/2$, U_{eff} the effective cooling velocity, and A, B, m, and n are the calibration constants.

The cold wire of the heat-flux probe is also calibrated in the laminar jet by varying the temperature of the flow and assuming that the resistance of the sensor is linearly related to temperature. An analytical technique has been developed to compensate the cold-wire measurements for frequency-response degradation due to the effect of wire thermal inertia and the effect of end conduction to the prongs. The method involves transforming the temperature time series into frequency space using a fast Fourier transform, spectrally compensating the measurements for both amplitude and phase shifting effects based on a predicted frequency-response curve, and recovering the compensated time series using an inverse transform method. The calibration procedure and compensation technique are described in more detail in ref. [17].

A correction was applied to the heat-flux terms to account for cross-flow contamination. When the probe is placed in a three-dimensional flow, or is not aligned properly in a two-dimensional flow, the cross component of mean velocity also contributes to U_{eff}. In particular, for the fluctuating part of the signal

$$u_{\text{eff}} = u\cos(\psi_{\text{eff}}) + v\sin(\psi_{\text{eff}}) + \frac{\bar{W}w}{\bar{U}\cos(\psi_{\text{eff}}) + \bar{V}\sin(\psi_{\text{eff}})} \quad (5)$$

where $\bar{W}$ is the mean cross component of velocity and ψ_{eff} the effective cooling angle [19]. This cross-flow contamination leads to errors in the Reynolds stresses and the turbulent heat fluxes. The correction was found to be very small (<1%) for the cross-plane heat fluxes ($\overline{v\theta}$ and $\overline{w\theta}$), because the contamination effect from each of the two wires of the X-wire tended to cancel. However, the correction was as high as 15% for the streamwise heat flux, $\overline{u\theta}$. No correction was applied to the Reynolds stresses, but was estimated to be a maximum of approximately 10% for both $\overline{uv}$ and $\overline{uw}$.

RESULTS AND DISCUSSION

Mean measurements and vortex characterization

The operating conditions used for this study are presented in Table 1 along with some characteristics of the boundary layer and vortex.

The mean streamwise velocity contours and the secondary flow vectors are shown in Fig. 2 for the y–z plane considered in this study ($x = 2.65$ m). Note that the data shown in this figure (and the remaining figures as well) are concentrated around the region of the vortex to capture the main interactions between the vortex and the boundary layer. No data were taken in the outer spanwise regions, which are generally characterized by a gradual return to two-dimensional behavior [4].

Table 1. Operating conditions and boundary-layer characteristics at $x = 2.65$ m

Operating conditions	
U_∞	$10.6\ \text{m s}^{-1}$
Re_x	1.82×10^6
q_w	$350\ \text{W m}^{-2}$
Undisturbed boundary-layer parameters	
Re_{δ_2}	3300
δ	4.2 cm
Δ	4.4 cm
$T_w - T_\infty$	15.2°C
u_τ	$0.41\ \text{m s}^{-1}$
St	0.00189
Vortex parameters	
Γ/U_∞	−0.72 cm
$(\Omega_z/U_\infty)_{\max}$	$-0.088\ \text{cm}^{-1}$

The general features shown in Fig. 2 are similar to those found in earlier studies [1, 4]. The boundary layer is thinned in the downwash region, where high momentum fluid from the free stream is convected towards the wall. Likewise, the boundary layer is thickened in the upwash region as low momentum fluid from near the wall is convected upwards. In the region near the core of the vortex, the gradients of streamwise velocity are small, indicating that the wake which usually forms directly behind the vortex generator [4] has diffused significantly. Outside the downwash region, the boundary-layer thickness, δ_{loc}, is returning towards its undisturbed two-dimensional value of 4.2 cm.

Stanton numbers were calculated from the wall-temperature measurements, and normalized on the Stanton numbers measured at the same location in the two-dimensional boundary layer. The results are similar to those of ref. [4], with a peak enhancement of nearly 25% in the region near the downwash side of the vortex.

The streamwise vorticity field, $\Omega_x = \partial\bar{W}/\partial y - \partial\bar{V}/\partial z$, is useful in characterizing the vortex, and is shown in Fig. 3. The gradients of the secondary velocities were determined by fitting a cubic spline to the velocity data at a given y or a given z location, and then analytically differentiating the spline curves. Near the core of the vortex the vorticity contours are nearly circular, which would be characteristic of a diffusing, free vortex. Near the upwash region, opposite sign vorticity is generated as a result of the no-slip conditions imposed by the wall on the vortex. Both of these characteristics have been observed in previous studies [4, 5]. Further out from the core, the vorticity con-

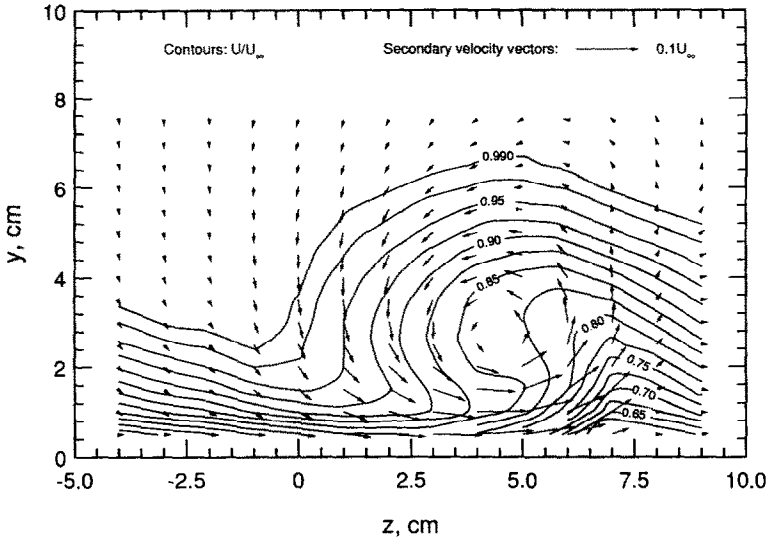

FIG. 2. Normalized streamwise velocity contours and secondary velocity vectors, $\bar{V}\hat{j}+\bar{W}\hat{k}$.

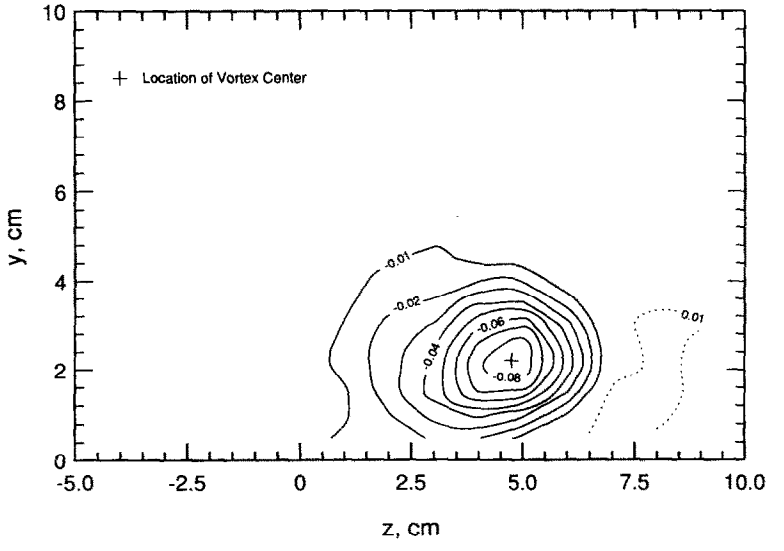

FIG. 3. Streamwise vorticity contours, $\Omega_x/U_\infty = (\partial\bar{W}/\partial y - \partial\bar{V}/\partial z)/U_\infty$ (in cm^{-1}).

tours become somewhat elliptical in shape, probably due to the limits imposed on diffusion by the presence of both the wall and the region of opposite sign vorticity.

Westphal *et al.* [3] suggested that three parameters be used to describe the vortex: location of the vortex as characterized by the center of the vorticity contours, peak vorticity, and circulation. From Fig. 3, the center of the vortex appears to be at $z = 4.8$ cm and $y = 2.2$ cm. Note that this does not usually correspond to the point where the secondary velocity vector is zero, because of the effect of the wall. That location, from Fig. 2, is approximately at $z = 4.2$ cm, $y = 2.8$ cm. The peak vorticity is $\Omega_x/U_\infty = -0.088$ cm^{-1}, although this could be low, because data was taken on a somewhat coarse grid. The circulation is $\Gamma/U_\infty = -0.72$ cm and was found using the technique similar to Westphal *et al.* [3], in which the vorticity field is integrated from the vortex center out to the contour which is 10% of the peak vorticity.

In summary, the vortex can be characterized as a relatively weak one, which has been somewhat distorted in shape due to asymmetrical diffusion. Velocity, vorticity, and Stanton number results are consistent with previous studies on similar strength vortices.

Turbulent heat fluxes and Reynolds stresses

Contour plots for the cross-plane heat fluxes, $\overline{v\theta}$ and $\overline{w\theta}$, are shown in Figs. 4 and 5, along with contours for

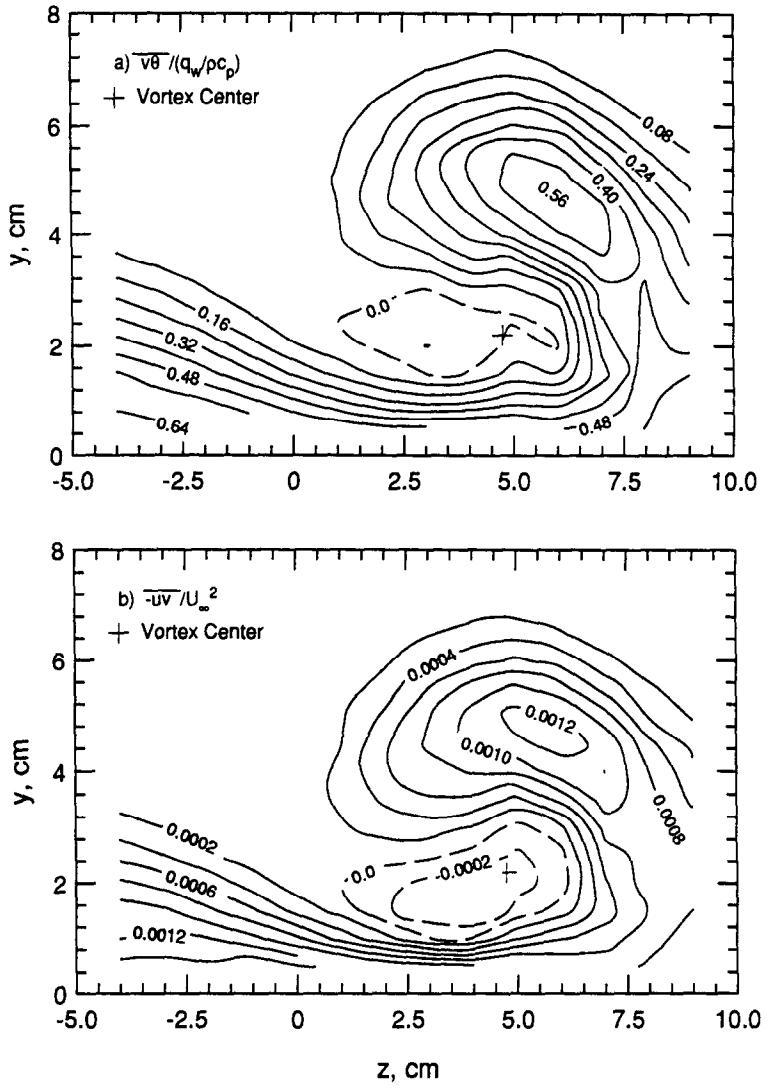

FIG. 4. (a) Normal component of turbulent heat flux, $\overline{v\theta}/(q_w/\rho c_p)$. (b) Reynolds shear stress, $\overline{uv}/U_\infty^2$.

the analogous Reynolds stress terms, $\overline{uv}$ and $\overline{uw}$. There is some similarity between the shapes of the $\overline{v\theta}$ and $\overline{uv}$ contours and of the $\overline{w\theta}$ and $\overline{uw}$ contours, indicating some rough analogy between momentum and heat transport. Both $\overline{v\theta}$ and $\overline{uv}$ (Fig. 4) exhibit a region of reversed sign near the vortex center, and a region of elevated values on the upwash side of the vortex consistent with convection of near wall fluid up into the flow. The contours of $\overline{w\theta}$ and $\overline{uw}$ (Fig. 5) both have a maximum near the wall in the upwash region, and reversals in signs approximately corresponding to locations where the spanwise gradients of the mean streamwise velocity also change sign. Despite these apparent gross similarities, differences do exist between turbulent momentum and heat transport, and these will be discussed below.

Figure 6 shows the contour plots for the temperature fluctuations, $(\theta')^2$, and the turbulent kinetic energy, k^2. These show similar behavior, with a finger of fluid characterized by high kinetic energy and high temperature fluctuations extending from the wall upwards into the upwash region and a similar region of low fluctuations extending down towards the wall in the downwash region. These profiles indicate that $(\theta')^2$ and k^2 are being transported primarily by passive convection as a result of the secondary flow [2]. The individual normal stress terms, not shown here, also follow this trend. However, as was also observed by Pauley and Eaton [5], the three Reynolds normal stresses ($(u')^2$, $(v')^2$, and $(w')^2$) are all nearly equal near the core of the vortex, suggesting an isotropic turbulence field in this region.

Contours of the streamwise turbulent heat flux, $\overline{u\theta}$, and its correlation coefficient are shown in Fig. 7. The behavior of $\overline{u\theta}$ looks qualitatively similar to that of $(\theta')^2$ or k^2. However, the correlation coefficient, which

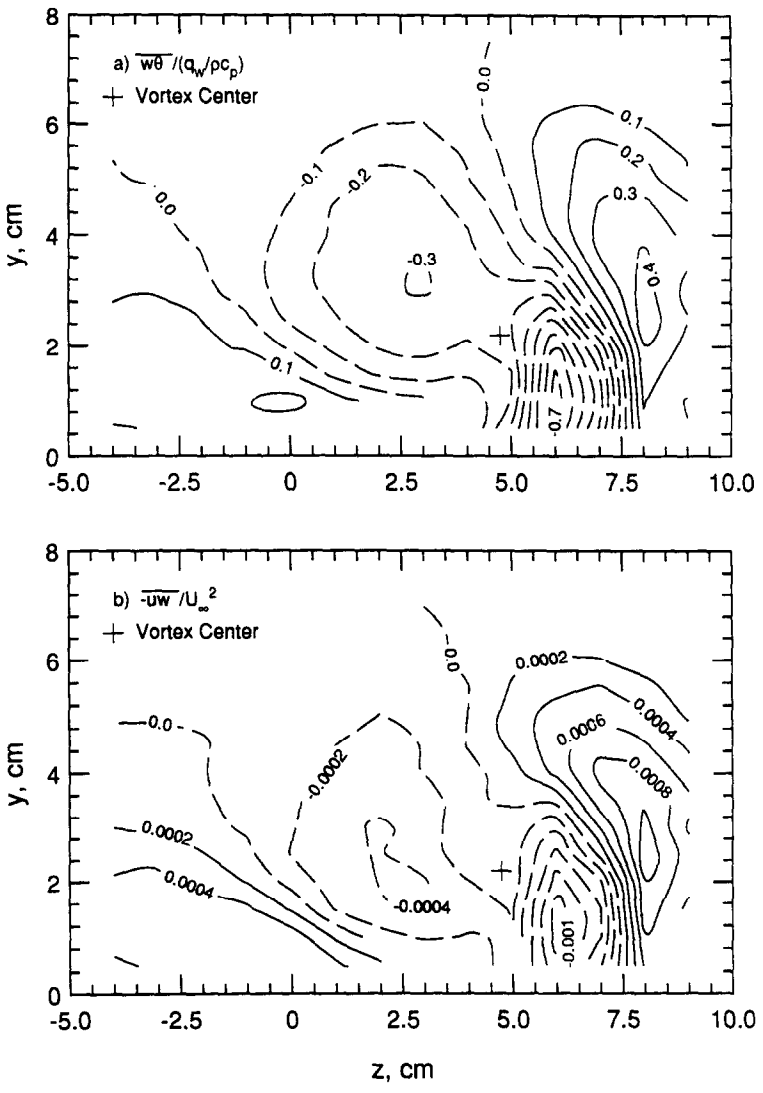

FIG. 5. (a) Spanwise component of turbulent heat flux, $\overline{w\theta}/(q_w/\rho c_p)$. (b) Reynolds shear stress, $-\overline{uw}/U_\infty^2$.

is nearly constant at 0.6 in the outer region of a two-dimensional boundary layer, is seen to be reduced significantly in the downwash and vortex-core regions. This suggests that the vortex is altering the mechanisms for streamwise turbulent heat transport in these areas of the flow. It is worthwhile to mention that the basic mechanism associated with $\overline{u\theta}$ is thought to be different from that associated with transport in the normal direction, $\overline{v\theta}$. In a two-dimensional boundary layer, and also in this flow as described below, $\overline{v\theta}$ is well approximated by a gradient-diffusion model, implying that heat is primarily transported by scales smaller than the length scales of the mean flow. On the other hand, $\overline{u\theta}$ is larger than $\overline{v\theta}$ (in a two-dimensional flow and in the vortex flow as well), even though the streamwise gradients are much smaller than the normal gradients. This suggests that larger, non-isotropic motions may be the dominant mechanisms for streamwise heat transport in the outer region. In support of this, spectral measurements of $\overline{u\theta}$ and $\overline{v\theta}$ were obtained in two-dimensional boundary layers, and these showed that $\overline{u\theta}$ has greater contributions from lower frequency fluctuations than $\overline{v\theta}$.

To further investigate the cross-plane heat fluxes, it is convenient to define a vector heat flux, which is formed by these two values, $\overline{v\theta}\hat{j}+\overline{w\theta}\hat{k}$, where $\hat{j}$ and $\hat{k}$ are unit vectors in the y and z directions. These vectors are plotted in Fig. 8 along with the mean temperature contours. For most of the locations within the boundary layer, the direction of the heat flux corresponds closely to the direction of the temperature gradient. This is true even in the region where the temperature gradients are negative. The implication of this result is that a gradient-diffusion model would be a good approximation for the turbulent heat flux in these flows.

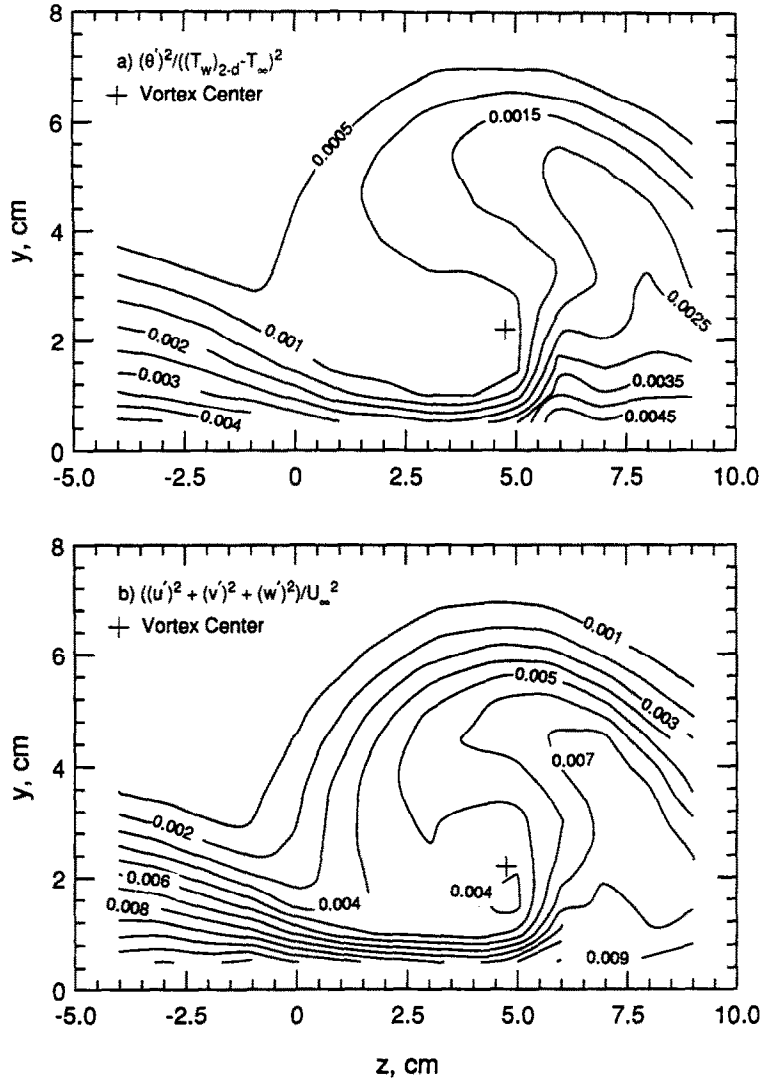

FIG. 6. (a) Temperature fluctuations, $(\theta')^2/[(T_w)_{2\text{-}d}-T_\infty]^2$, where $(T_w)_{2\text{-}d} = T_w(z = -22.3)$. (b) Turbulent kinetic energy, $k^2/U_\infty^2 = [(u')^2+(v')^2+(w')^2]/U_\infty^2$.

It should be noted, however, that there are a few areas in the flow that deviate from the ideal behavior. In particular, in the region near the wall at $z = 6$, the differences in vector directions are as high as 30 deg, which is larger than what would be expected purely from experimental uncertainty. In these regions, a gradient-diffusion model may be questionable, and a convective velocity component of the transport may be required. Despite these few questionable regions, the heat-flux data will be further evaluated by assuming that the heat-flux vector and temperature-gradient vector do align. The benefits of such a straightforward approach hopefully outweigh the fact that it may not be fully valid in a few specific areas of the flow.

Figure 9 shows a similar plot for the cross-plane momentum-flux vectors, $-\overline{uv}\hat{j}-\overline{uv}\hat{k}$. For most of the flow field, the momentum-transport vector also aligns well with the mean streamwise velocity gradient. However, there seem to be more areas that deviate from this behavior than in the case of the heat transport (Fig. 8), most notably in the region directly above the vortex core. Shabaka *et al.* [1] reported a negative spanwise eddy viscosity in this region, which is consistent with the behavior observed in Fig. 9. In addition, Johnston [20] reported that in three-dimensional shear layers, the shear-stress vector did not align with the vector of the mean velocity gradient. So, some experimental evidence does exist that supports the conclusion that the momentum transport and mean-velocity-gradient vector may, in general, have different orientations.

Shabaka *et al.* [1] and Pauley and Eaton [5] found that the Reynolds stresses were very small near the core of the vortex, despite relatively high turbulence levels, indicating that turbulent transport of momen-

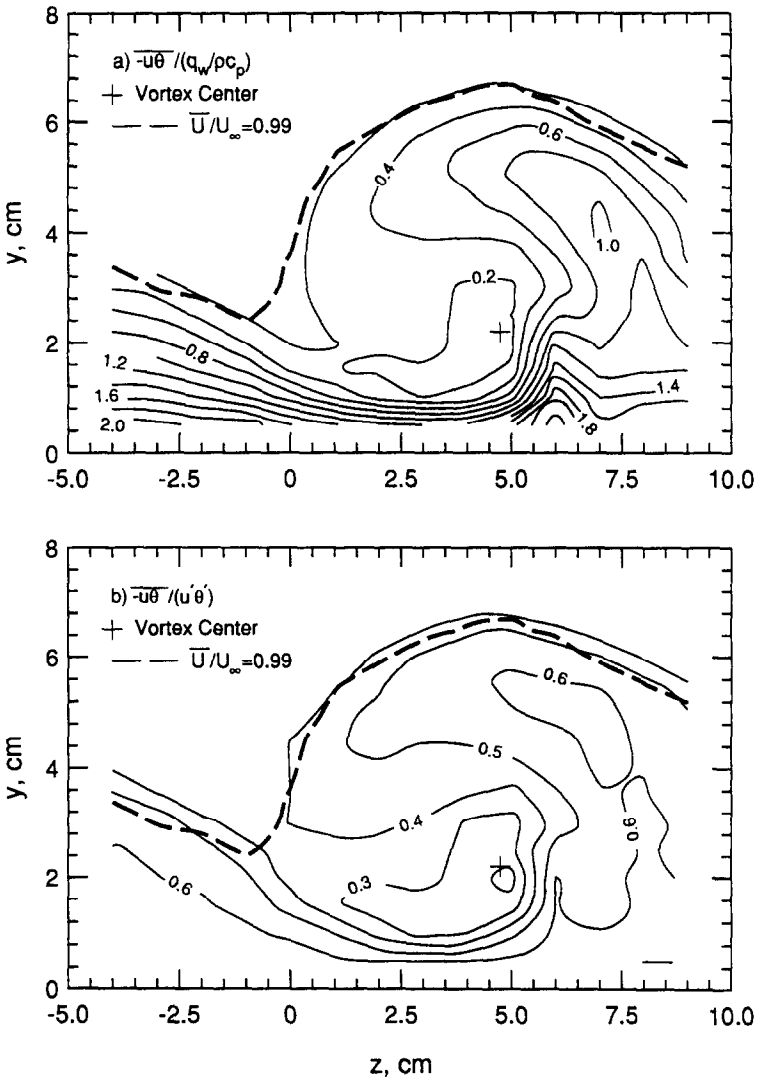

FIG. 7. (a) Streamwise component of turbulent heat flux, $-u\theta/(q_w/\rho c_p)$. (b) Correlation coefficient, $-\overline{u\theta}/(u'\theta')$.

tum was suppressed. This is also seen in the present results in Fig. 9. However, the heat flux, which is predominantly in the z-direction as a result of the skewing of the temperature contours, is not suppressed in this region, suggesting a significant difference between passive-scalar transport and momentum transport in the core region of the vortex. It is interesting to note that, in the downwash region, the thermal boundary layer is not thinned as much as the momentum boundary layer. This can be seen by comparing the mean temperature and mean velocity contours in Figs. 8 and 9. For example, at $z = -1$, the thermal boundary layer is about 50% larger than the momentum boundary layer. (In the two-dimensional case, the thermal boundary layer is also larger than the momentum boundary layer, but only by about 5%.) This difference could be due to the greater level of turbulent diffusion of heat compared to momentum near the core. This will be discussed further below in connection with the turbulent Prandtl number.

The cross-plane vector heat flux can also be used to define a structure parameter, $a_\theta = [(\overline{v\theta})^2 + (\overline{w\theta})^2]^{1/2}/[(\theta')^2 k^2]^{1/2}$, which is similar to a correlation coefficient, but uses k as the characteristic velocity rather than the individual r.m.s. velocities. This parameter is slightly modified from the one defined by Townsend [21] who included only the $\overline{v\theta}$ term for two-dimensional applications. The structure parameter may be interpreted as a relative measure of the ability of a certain level of turbulence to transport heat. In this sense, it is analogous to the stress-intensity ratio, $a_1 = |\tau|/k^2$, where $\tau = \overline{uv}$ for two-dimensional flows, and $\tau = (\overline{uv}^2 + \overline{vw}^2)^{1/2}$ for the vortex boundary-layer flow.

Figure 10 shows the contours of a_θ. For comparison, a_θ is approximately constant across the outer

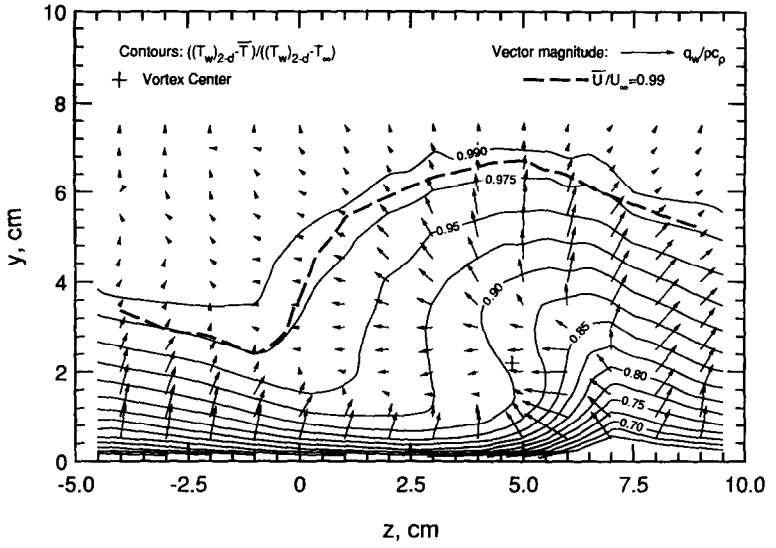

FIG. 8. Normalized temperature contours and cross-plane heat-flux vectors, $\overline{v\theta}\hat{j}+\overline{w\theta}\hat{k}$.

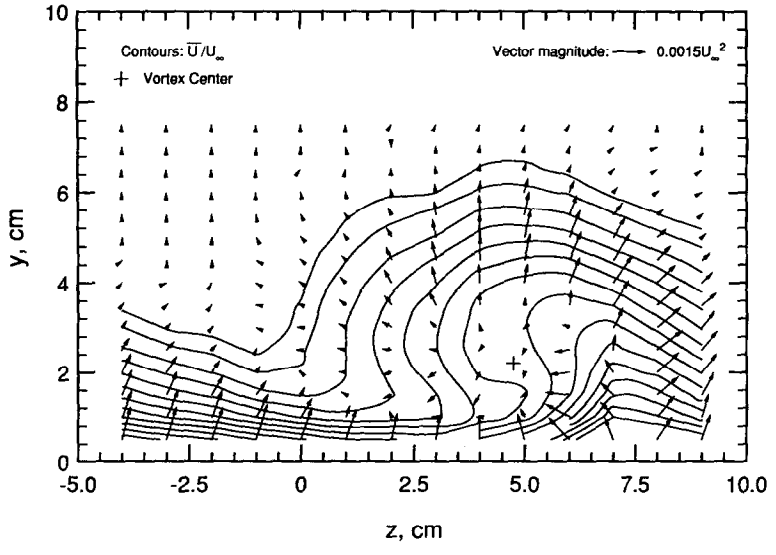

FIG. 9. Normalized streamwise velocity contours and cross-plane momentum-flux vectors, $-(\overline{uv}\hat{j}+\overline{uw}\hat{k})$.

region of a two-dimensional boundary layer, and has a value of approximately 0.22. This is consistent with the values shown in Fig. 10 for the outer spanwise region on the downwash side, which is nearly two-dimensional. However, in the region of the vortex, the values differ significantly, indicating that the vortex has altered the structure of the turbulence. In particular, a significant portion of the region above the vortex core shows elevated values of a_θ, which are as much as 50% higher than in a two-dimensional flow. This may be interpreted as an increased ability of the turbulent fluctuations to transport heat. There is also a region near the downwash side, where a_θ is lower than the corresponding two-dimensional value. This region is characterized by very small temperature gradients and very low heat fluxes, suggesting that the reduced values of a_θ may be due to experimental uncertainty.

The idea that the vortex drastically alters the turbulent structure was reported by both Shabaka *et al.* [1] for the single vortex, who presented a_1 data with only the $\overline{uv}$ term included, and by Pauley and Eaton [5] for vortex pairs, who reported a_1 with both $\overline{uv}$ and $\overline{vw}$. However, in both cases, values of a_1 were mostly less than or equal to the corresponding two-dimensional values. This seems to indicate that the changes in the turbulence structure brought about by the vortex favor enhanced transport of heat compared to momentum.

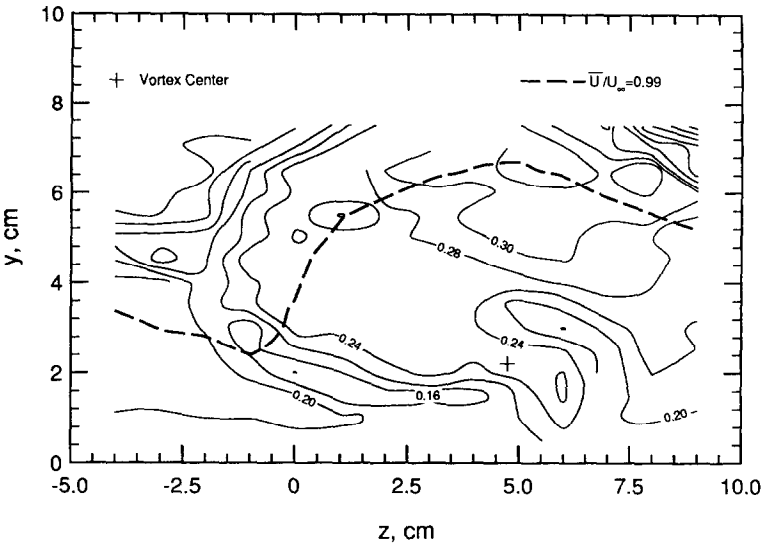

FIG. 10. Heat-flux structure parameter, $a_0 = [(\overline{v\theta})^2 + (\overline{w\theta})^2]^{1/2}/[\theta'(k^2)^{1/2}]$.

Eddy diffusivity and turbulent Prandtl number

The alignment of the cross-plane heat-flux vector and the temperature-gradient vector has major implications on the form of the eddy diffusivity. In the most general sense, the diffusivity is expressed as a second-order tensor, $\mathscr{D}_{ij}$ [22]

$$\overline{u_i\theta} = \mathscr{D}_{ij}\frac{\partial \tilde{T}}{\partial x_j}. \tag{6}$$

Here, index notation has been used for brevity (i.e. $\overline{u_2\theta} = \overline{v\theta}$, $x_2 = y$, etc.). Since the streamwise gradients are expected to be small, and since $\overline{u\theta}$ may not be well approximated by a gradient diffusion model, equation (6) can be reduced to

$$\overline{v\theta} = \mathscr{D}_{22}\frac{\partial \tilde{T}}{\partial y} + \mathscr{D}_{23}\frac{\partial \tilde{T}}{\partial z} \tag{7}$$

$$\overline{w\theta} = \mathscr{D}_{32}\frac{\partial \tilde{T}}{\partial y} + \mathscr{D}_{33}\frac{\partial \tilde{T}}{\partial z} \tag{8}$$

where the original notation has now been used. From this, the cross-plane vector heat flux may now be expressed as

$$\overline{v\theta}\hat{j} + \overline{w\theta}\hat{k} = \left(\mathscr{D}_{22}\frac{\partial \tilde{T}}{\partial y} + \mathscr{D}_{23}\frac{\partial \tilde{T}}{\partial z}\right)\hat{j} + \left(\mathscr{D}_{32}\frac{\partial \tilde{T}}{\partial y} + \mathscr{D}_{33}\frac{\partial \tilde{T}}{\partial z}\right)\hat{k}. \tag{9}$$

The alignment of the heat-flux and temperature-gradient vectors implies that

$$\overline{v\theta}\hat{j} + \overline{w\theta}\hat{k} = \varepsilon_H\left(\frac{\partial \tilde{T}}{\partial y}\hat{j} + \frac{\partial \tilde{T}}{\partial z}\hat{k}\right) \tag{10}$$

where ε_H must be a scalar that can be a function of location. The only way that equations (9) and (10) can both be valid is if $\mathscr{D}_{23} = \mathscr{D}_{32} = 0$ and $\varepsilon_H = \mathscr{D}_{22} = \mathscr{D}_{33}$. So, for the cross-plane heat fluxes, the eddy-diffusivity tensor reduces to a scalar value.

Given the scalar form of the eddy diffusivity, it is then logical to define it by using the vectors of the heat flux and temperature gradients

$$\varepsilon_H = \frac{[(\overline{v\theta})^2 + (\overline{w\theta})^2]^{1/2}}{[(\partial\tilde{T}/\partial y)^2 + (\partial\tilde{T}/\partial z)^2]^{1/2}}. \tag{11}$$

Defining the diffusivity in this sense reduces the possibility of extreme or negative values in regions where either $\overline{v\theta}$ or $\overline{w\theta}$ are small. However, it should also be noted that this definition effectively forces an isotropic eddy diffusivity for the few locations in which the agreement between the direction of the heat-flux vector and temperature-gradient vector may be questionable.

Figure 11 shows contours of the eddy diffusivity as defined by equation (11), normalized by the free-stream velocity and the undisturbed, two-dimensional boundary-layer thickness. (The choice of the two-dimensional boundary-layer thickness as the appropriate length scale is basically a convenience to allow all the results to be scaled on the same value.) The eddy diffusivity in the area to the left of the downwash region is again consistent with two-dimensional boundary-layer behavior, where values are between 0.0025 and 0.003. In the region above and to the sides of the vortex, the eddy diffusivities are larger than those in the two-dimensional flow. In particular, the eddy diffusivity is as much as two times higher in the downwash region. Part of this effect may be due to the increase in the local boundary-layer thickness in that region.

In the most general sense, the eddy diffusivity is a second-order tensor, $\mathscr{D}_{ij}$, and the eddy viscosity may be either a fourth- or second-order tensor, depending upon whether the normal stresses need to be con-

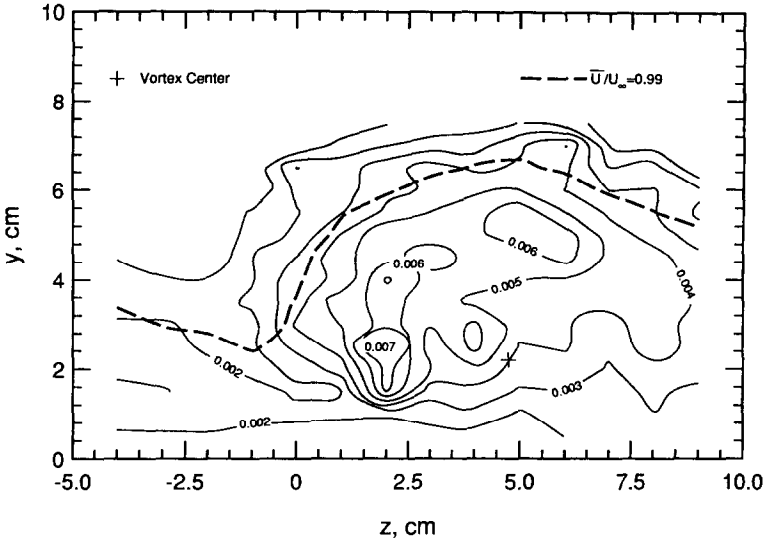

FIG. 11. Isotropic eddy diffusivity, $\varepsilon_H/(U_\infty\delta_{2\text{-d}})$, where $\varepsilon_H = [(\overline{v\theta})^2+(\overline{w\theta})^2]^{1/2}/[(\partial\bar{T}/\partial y)^2+(\partial\bar{T}/\partial z)^2]^{1/2}$.

sidered [22]. Considering the simpler case of a second-order eddy-viscosity tensor, $\mathscr{V}_{ij}$, a turbulent Prandtl number tensor may be defined

$$\mathscr{V}_{ij} = \mathscr{P}_{ik}\mathscr{D}_{kj}. \tag{12}$$

For this general case, the physical meaning of the individual terms of the $\mathscr{P}_{ik}$ tensor are lost, and so its usefulness from a modeling standpoint.

If we assume that the eddy diffusivity and the eddy viscosity are diagonal tensors, then the Reynolds shear stresses can be expressed as

$$\overline{uw} = \mathscr{V}_{22}\frac{\partial\bar{U}}{\partial y} \tag{13}$$

$$\overline{uw} = \mathscr{V}_{33}\frac{\partial\bar{U}}{\partial z} \tag{14}$$

$$\overline{vw} = \mathscr{V}_{33}\left(\frac{\partial\bar{V}}{\partial z}+\frac{\partial\bar{W}}{\partial y}\right). \tag{15}$$

With this simplification, and by neglecting the $\mathscr{V}_{11}$ and $\mathscr{D}_{11}$ terms (since it is not expected that $(u')^2$ and $\overline{u\theta}$ will be approximated by gradient diffusion), the turbulent Prandtl number tensor reduces to two scalar values

$$\mathscr{P}_{22} = \frac{\mathscr{V}_{22}}{\mathscr{D}_{22}} \tag{16}$$

$$\mathscr{P}_{33} = \frac{\mathscr{V}_{33}}{\mathscr{D}_{33}}. \tag{17}$$

In this greatly simplified form, these ratios do take on some physical significance as directional turbulent Prandtl numbers. For example, $\mathscr{P}_{22}$, which is the familiar form for two-dimensional boundary layers, can be thought of as a relative measure of the ability of the turbulence to transport streamwise momentum compared to heat in the y-direction.

It has been shown already that the eddy diffusivity can be approximated as a scalar quantity for most of the flow region. It seems uncertain whether the same assumption may be made for the eddy viscosity, based on the above discussion. However, for purposes of comparison, the eddy viscosity will be approximated as isotropic, $\varepsilon_M = \mathscr{V}_{22} = \mathscr{V}_{33}$, with the caveat that this is probably not true for all regions of the flows. With this convenient definition, a scalar turbulent Prandtl number can be defined in the usual way

$$Pr_t = \frac{\varepsilon_M}{\varepsilon_H}. \tag{18}$$

Contours of Pr_t are shown in Fig. 12. In the outer spanwise regions, the inner region below the vortex, and the upwash region, the turbulent Prandtl number is within the expected range of 0.8–1.2 for two-dimensional boundary layers. The vortex-core region and the downwash region, where the transport is predominantly in the z-direction, are characterized by significantly lower turbulent Prandtl numbers. This is consistent with the observation that momentum transport is suppressed near the core but heat transport is not. The turbulent diffusion of heat in this region, which opposes mean convection by strong secondary velocities in the downwash region, may explain why the thermal boundary layer is thicker than the momentum boundary layer in the area near $z = -1$. Above the vortex, where the transport is predominantly in the y-direction, Pr_t is about 25% lower than the two-dimensional levels. Although this is only slightly larger than the uncertainties (18%), the trend does support the contention that the effect of the vortex is to enhance heat transport more than momentum transport in this area.

As shown above, a meaningful definition of turbulent Prandtl number arises only with the assump-

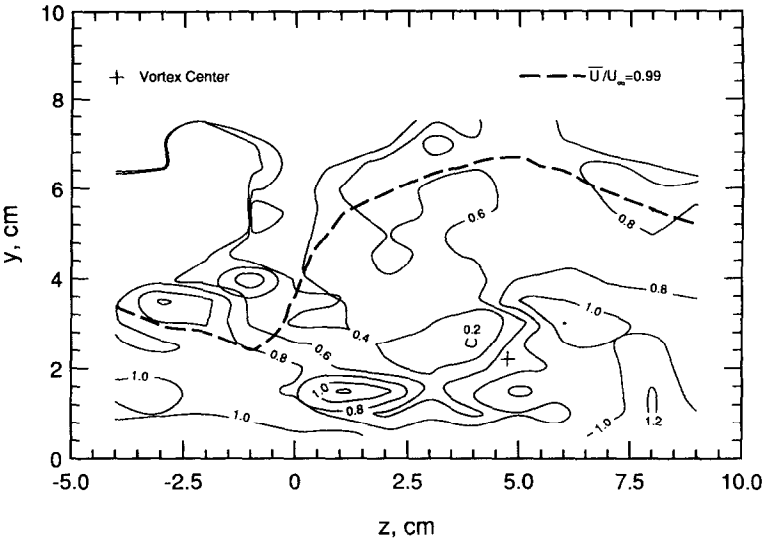

FIG. 12. Turbulent Prandtl number, $\varepsilon_M/\varepsilon_H$.

tion of diagonal eddy-viscosity and eddy-diffusivity tensors. While this study has shown that to be valid for the diffusivity, it is not clear whether this assumption can be made for the viscosity. In addition, the main usefulness of the turbulent Prandtl number is as a modeling tool, to allow for estimation of the turbulent heat-flux terms, once an appropriate model for the Reynolds stresses has been devised. Previous studies [1, 2] indicate that higher order turbulence models are required to adequately predict the Reynolds stresses, and the results presented here suggest that a gradient-diffusion model could be devised to model the heat flux. Therefore, attempting to define some convenient turbulent Prandtl number for modeling purposes may only add an unnecessary complexity to the heat-transfer problem.

CONCLUSIONS

All three turbulent heat-flux terms have been measured in a boundary layer disturbed by a relatively weak embedded streamwise vortex. Some gross similarities exist between analogous heat-flux and Reynolds stress terms. However, the changes to the turbulence structure caused by the vortex seem to favor enhanced heat transport compared to momentum. In particular, the region near the vortex core, which was thought to be an area of suppressed diffusion of momentum, appears to be an area where heat transport is somewhat enhanced, mostly due to z-direction diffusion. The thermal boundary layer appears to spread further than the momentum boundary layer in the downwash region, in opposition to the strong mean convective transport imposed by the vortex. This is consistent with the idea that turbulent heat transport is enhanced compared to momentum transport in that region.

The cross-plane heat fluxes, $\overline{v\theta}$ and $\overline{w\theta}$, are nearly perpendicular to the isotherms at all locations, suggesting that a gradient-diffusion model with an isotropic eddy diffusivity would be appropriate. A meaningful turbulent Prandtl number can be defined only if some simplifying assumptions are made regarding the form of the eddy viscosity. This is useful in supporting some of the observed behavior of the flow, but it is not recommended as a modeling tool for this class of flows.

Acknowledgements—Funding for this work was provided by the Department of Energy Office of Basic Energy Science under contract number DE-FG03-87ER13780, and monitored by Dr Oscar Manley.

REFERENCES

1. I. M. M. A. Shabaka, R. D. Mehta and P. Bradshaw, Longitudinal vortices imbedded in turbulent boundary layers, *J. Fluid Mech* **155**, 37–57 (1985).
2. R. D. Mehta, I. M. M. A. Shabaka, A. Shibl and P. Bradshaw, Longitudinal vortices imbedded in turbulent boundary layers, AIAA-83-0378 (1983).
3. R. V. Westphal, J. K. Eaton and W. R. Pauley, Interaction between a vortex and a turbulent boundary layer in a streamwise pressure gradient. In *Turbulent Shear Flows* 5 (Edited by F. Durst, B. E. Launder, J. L. Lumley, F. W. Schmidt and J. H. Whitelaw), pp. 266–277. Springer, Berlin (1987).
4. P. A. Eibeck and J. K. Eaton, An experimental investigation of the heat-transfer effects of a longitudinal vortex embedded in a turbulent boundary layer, Report MD-48, Thermosciences Division, Department of Mechanical Engineering, Stanford University (1985).
5. W. R. Pauley and J. K. Eaton, The fluid dynamics and heat transfer effects of streamwise vortices embedded in a turbulent boundary layer, Report MD-51, Thermosciences Division, Department of Mechanical Engineering, Stanford University (1988).
6. J. Blom, Experimental determination of the turbulent Prandtl number in a developing temperature boundary

layer, *Heat Transfer* 1970: *Papers Presented at the Fourth Int. Heat Transfer Conf., Paris Versailles*, 1970 (Edited by U. Grigull and E. Hahne), Vol. 1, Paper No. FC2.2. Elsevier, Amsterdam (1970).
7. I. J. Kestin and P. D. Richardson, Heat transfer across turbulent, incompressible boundary layers, *Int. J. Heat Mass Transfer* **6**, 147–189 (1963).
8. D. S. Johnson, Velocity and temperature fluctuation measurements in a turbulent boundary layer downstream of a stepwise discontinuity in wall temperature, *J. Appl. Mech.* **26**, 325–336 (1959).
9. B. F. Blackwell, W. M. Kays and R. J. Moffatt, The turbulent boundary layer on a porous plate. An experimental study of the heat transfer behavior with adverse pressure gradients, Report HMT-16, Thermosciences Division, Department of Mechanical Engineering, Stanford University (1972).
10. A. F. Orlando, W. M. Kays and R. J. Moffatt, Turbulent transport of heat and momentum in a boundary layer subject to deceleration, suction, and variable wall temperature, Report HMT-17, Thermosciences Division, Department of Mechanical Engineering, Stanford University (1974).
11. M. M. Pimenta, W. M. Kays and R. J. Moffatt, The turbulent boundary layer. An experimental study of the transport of momentum and heat with the effect of roughness, Report HMT-21, Thermosciences Division, Department of Mechanical Engineering, Stanford University (1975).
12. A. E. Perry and P. H. Hoffman, An experimental study of turbulent convection heat transfer from a flat plate, *J. Fluid Mech.* **77**, 355–368 (1976).
13. R. A. Antonia, H. Q. Danh and A. Prabhu, Response of a turbulent boundary layer to a step change in surface heat flux, *J. Fluid Mech.* **80**, 153–177 (1977).
14. C. S. Subramanian and R. A. Antonia, Effect of Reynolds number on a slightly heated boundary layer, *Int. J. Heat Mass Transfer* **24**, 1833–1846 (1981).
15. M. M. Gibson and C. A. Verriopoulos, Turbulent boundary layer on a mildly curved surface: Part 2: temperature field measurements, *Exp. Fluids* **2**, 73–80 (1984).
16. J. Kim and T. W. Simon, Measurements of the turbulent transport of heat and momentum in convexly curved boundary layers: effects of curvature, recovery, and free stream turbulence, ASME Paper 87-GT-199 (1987).
17. D. E. Wroblewski and P. A. Eibeck, A frequency-response compensation technique for cold wires and its application to a heat-flux probe, *Exp. Thermal Fluid Sci.* (1991), in press.
18. D. C. Collis and M. J. Williams, Two-dimensional convection from heated wires at low Reynolds numbers, *J. Fluid Mech.* **6**, 357–384 (1959).
19. P. Bradshaw, *An Introduction to Turbulence and its Measurement*, pp. 119–123. Pergamon Press, Oxford (1971).
20. J. P. Johnston, Experimental studies in 3-dimensional turbulent boundary layers, Report MD-34, Thermosciences Division, Department of Mechanical Engineering, Stanford University (1976).
21. A. A. Townsend, *The Structure of Turbulent Shear Flow*, 2nd Edn, pp. 356–360. Cambridge University Press, Cambridge (1976).
22. J. O. Hinze, *Turbulence*, 2nd Edn, pp. 22 26. McGraw-Hill, New York (1975).

MESURE DU TRANSFERT TURBULENT DE CHALEUR DANS UNE COUCHE LIMITE AVEC VORTEX DANS LE COEUR DE L'ECOULEMENT

Résumé—Les trois composantes du vecteur flux thermique turbulent ($\overline{u\theta}$, $\overline{v\theta}$, et $\overline{w\theta}$) et la plupart des composantes du tenseur de Reynolds sont mesurées dans une couche limite perturbée par un vortex dans le coeur de l'écoulement. On observe quelques similitudes entre $\overline{v\theta}$ et $\overline{w\theta}$ et les termes homologues $\overline{uv}$ et $\overline{uw}$. Néanmoins l'interaction du vortex avec la couche limite semble accroitre le transfert de chaleur plus que le transfert de quantité de mouvement, spécialement au voisinage du noyau tourbillonnaire. Le vecteur formé par $\overline{v\theta}$ et $\overline{w\theta}$ est presque perpendiculaire aux isothermes en tous les points, ce qui suggère que le modèle à diffusivité turbulente isotrope est convenable pour cet écoulement.

MESSUNG DES TURBULENTEN WÄRMEÜBERGANGS IN EINER GRENZSCHICHT MIT EINGELAGERTEM LÄNGSWIRBEL

Zusammenfassung—Es werden alle drei Komponenten des turbulenten Wärmestromdichten-Vektors ($\overline{u\theta}$, $\overline{v\theta}$, $\overline{w\theta}$) sowie die meisten Komponenten des Tensors der Reynolds-Spannungen in einer Grenzschicht gemessen, welche durch einen Längswirbel gestört ist. Es sind einige Ähnlichkeiten zwischen den Wärmestromdichten in Querrichtung ($\overline{v\theta}$, $\overline{w\theta}$) und den analogen Termen der Reynolds-Spannungen ($\overline{uv}$, $\overline{uw}$) zu beobachten. Allerdings scheint der Einfluß des Wirbels auf die Grenzschicht den Wärmetransport stärker zu verbessern als den Impulstransport—insbesondere in der Nähe des Wirbelkerns. Der Wärmetransport-Vektor in einer Ebene quer zur Strömungsrichtung (gebildet aus $\overline{v\theta}$ und $\overline{w\theta}$) ist an allen Punkten nahezu senkrecht zu den Isothermen. Dies deutet darauf hin, daß ein isotropes Turbulenzmodell mit Scheindiffusions-Koeffizienten für diese Strömung geeignet ist.

ИЗМЕРЕНИЕ ТУРБУЛЕНТНОГО ТЕПЛОПЕРЕНОСА В ПОГРАНИЧНОМ СЛОЕ ПРИ НАЛИЧИИ В НЕМ ПРОДОЛЬНОГО ВИХРЯ

Аннотация—Измеряются три компонента вектора турбулентного теплового потока ($\overline{u\theta}$, $\overline{v\theta}$ и $\overline{w\theta}$), а также большая часть компонентов рейнольдсовского тензора напряжения в пограничном слое, возмущенном погруженным продольным вихрем. Наблюдается некоторое сходство между тепловыми потоками в поперечной плоскости ($\overline{v\theta}$ и $\overline{w\theta}$) и аналогичными компонентами рейнольдсовского напряжения ($\overline{uv}$ и $\overline{uw}$). Однако взаимодействие вихря с пограничным слоем, по-видимому, больше усиливает теплоперенос, чем перенос импульса, особенно в окрестности ядра вихря. Вектор теплопереноса в поперечной плоскости, образованный $\overline{v\theta}$ и $\overline{w\theta}$, почти перпендикулярен изотермам во всех точках, что позволяет предположить адекватность изотропной модели вихревой диффузии для рассматриваемого течения.